Reusable radiographic image plates: analysis of response variations

Brendt Wohlberg (T-CNLS), Gary Sandine (X-8), Kevin Vixie (X-8), Kevin Buescher (X-8), Alexander Saunders (P-25)

May 8, 2001

Abstract

Reusable radiographic image plates, originally designed for X-ray applications, are used for proton radiography at the LANSCE PRAD facility. Digital images are recovered from the plates using a laser-based scanner, after which the plates are "erased" by exposure to a bright light source. It appears, from inspection of images recovered from multiple plates exposed to the same proton beam, that there are significant variations in plate response to radiation. An accurate characterization of such response variations is important in obtaining accurate measurements of the radiation image to which the plates are exposed. We propose a simple model of non-uniform plate response and use it to analyze experimental data. Our results suggest that the combined plate-scanner system varies (spatially) in its response by up to 7%, and that the assumption of a static, spatially varying image plate response explains at most 50% of the observed variation in response. While these results show that the model we used is not able to explain all the observed variations adequately, we believe our model to be the correct first step in an effort aimed at providing a complete explanation of the experiments. Whether or not this study is continued should depend on whether or not the plates will be used in the future.

1 Introduction

Reusable radiographic image plates, originally designed for X-ray applications, are used for proton radiography at the LANSCE PRAD facility. Digital images are recovered from the plates using a laser-based drum scanner, after which the plates are "erased" by exposure to a bright light source. The delay between exposure and scanning is significant since the images recorded on the plates decay with time. The plates are usually scanned at 150 dpi, resulting in 1100×750 pixel (width $\times$ height) images, each pixel having a width and height of approximately 0.17mm.

The plates are placed directly in the beam line during exposure. A stack of 4 plates is usually used, the scanned images being averaged in an attempt to obtain a more accurate final representation of the radiation image within the beam. Comparison of the images (after alignment using fiducial marks) from plates exposed in the same stack reveal significant differences which do not appear to arise from the expected random noise. Consider Figure 1(a), which represents the ratio of the images from two plates exposed simultaneously; the observed pattern suggests highly correlated variations in gain across the plates rather than white noise fluctuations. Comparison with Figure 1(b), however, reveals that these patterns of gain variation are not particularly stable from one exposure to the next. (The horseshoe shaped region of consistency corresponds roughly to the area of maximum beam intensity; this observation is addressed in more detail later in this report.)

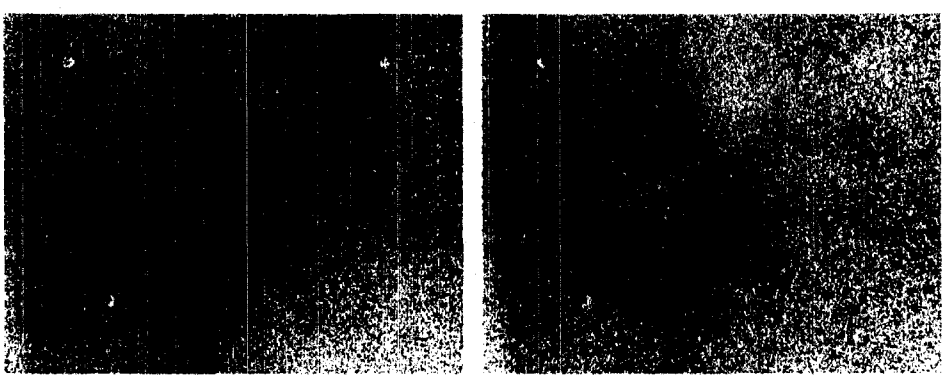

(a) Run 11451 (b) Run 11455

Figure 1: Ratios of plate A6 to plate A31 for two different exposures. The black regions have values below 0.95, and the white regions have values above 1.05.

An accurate characterization of these response variations is important in obtaining accurate measurements of beam images. The two main potential sources for these variations are (i) spatial non-uniformities in image plate response, and (ii) variations arising during the scanning process, due, for example, to small differences in the mounting of plates on the scanner drum. We have analyzed these variations using experimental data[1] collected at the LANL LANSCE Line C PRAD facility during the last quarter of 2000.

The first set of experimental data, the analysis of which is discussed in the following two sections, consisted of a set of 4 plates, which were simultaneously exposed to the proton beam for 4 different experimental runs. These data were used in an attempt to characterize spatial radiation response or gain patterns for each plate. The second set consisted of a set of plates which had been inscribed with a regular grid pattern, for use in examining distortions arising during scanning. The analysis of these data is discussed in Section 4.

2 A Simple Model of Spatial Variations

We have plate scans for multiple plates, exposed during multiple experimental runs. We consider the simple model[2]

$$S_{p,r} = \alpha_{p,r} B_r \odot G_p,$$

where $S_{p,r}$ represents the scan of plate number p exposed during run number r, B_r represents the beam to which all plates were exposed during run r, G_p represents a gain image for plate p, and $\alpha_{p,r}$ is a scalar representing the decay in scan intensity due to variable delays between exposure and scanning. Note that this model ignores the position of a plate in the stack of plates exposed to the same beam, and assumes that the response of each plate may be characterized by a constant-in-time scalar gain at each plate position.

While the $\alpha_{p,r}$ values could be estimated from records of exposure and scan times, we consider them unknowns for the purposes of this report; all plate scans are normalized prior to analysis, and the beam and gain images are only estimated up to an unknown scaling factor. The model thus becomes

$$S'_{p,r} = B'_r \odot G'_p,$$

where $S_{p,r}$ is the normalized plate scan, and B'_r and G'_p are beam and gain images which are meaningful up to an unknown scaling factor.

[1] While additional data were collected, only the data used for analysis described in this report are discussed here.

[2] The Hadamard product $C = A \odot B$ of matrices A and B is defined as $c_{m,n} = a_{m,n} b_{m,n}$.

This model represents an overdetermined system for the numbers of plates and runs of interest (for example, 4 plates, 4 runs); we find best-fit B'_r and G'_p images by least-squares optimization.

3 Data Analysis

Plate scans were aligned (using fiducial marks in each image) and cropped before averaging pixel values in 32×32 blocks to reduce noise and computational requirements of the optimization procedure to follow. A non-linear least squares optimization was then applied to find best-fit B'_r and G'_p for the $S'_{p,r}$ images obtained as described. The initial solution for the gradient descent algorithm was obtained by setting G'_p to 1.0 at all pixels, and setting B'_r to an average of the scans for the plates used in run r. The specific distance measure minimized was $\sum_{p,r} \|S'_{p,r} - B'_r \odot G'_p\|$.

Resulting low resolution gain estimates are displayed in Figures 2 to 5. While the optimization found a reasonable fit to the model (with very similar beam profiles B'_r), it should be noted that the solution is not necessarily a global minimum. The optimization was furthermore found to be sensitive to initial solution and the precise form of the distance measure; a number of alternative settings found solutions which were not physically reasonable.

These best fit results are of rather limited utility without a measure of the accuracy with which the model describes the data. We constructed such a measure by comparing, for each plate, separate gain estimates obtained from each run. Individual gain estimates for each run were then calculated as[3]

$$\tilde{G}_{p,r} = S'_{p,r} / B'_r.$$

For each plate, a standard deviation over all runs was calculated at each point in the gain image, and a final standard deviation averaged over the entire image was calculated as a measure of the stability of the gain image from one run to the next. For purposes of comparison, a spatial standard deviation was calculated as a measure of "strength" of the gain pattern for each gain image G'_p. The resulting standard deviations are tabulated in Table 1. Note that the gain variation between runs is of similar magnitude to the gain variation across each plate - apparently the model does not fit the data well.

It may be observed, however, that the across-run standard deviation varies significantly across each gain image, with a low variance where the beam is strong, and a much higher variance where the beam is weak (see Figures 6 and 7). Restricting the analysis described previously to the small region of peak beam intensity gives

[3]Where $C = A/B$ denotes division such that $c_{m,n} = a_{m,n}/b_{m,n}$.

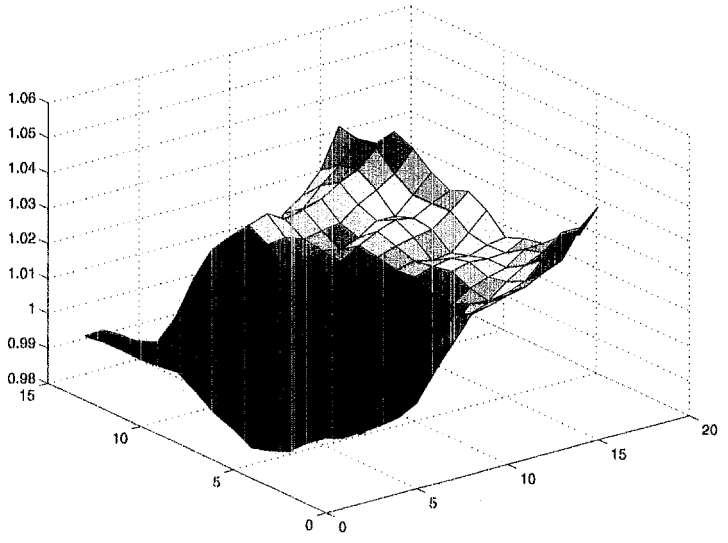

Figure 2: Estimated gain image for plate A6.

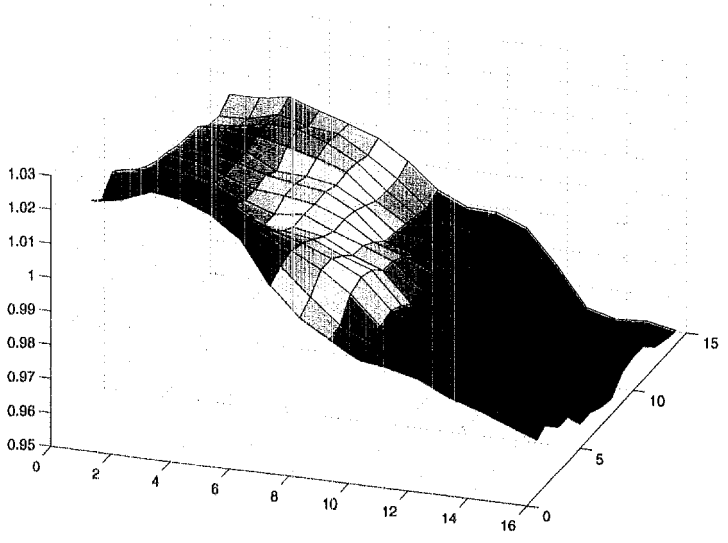

Figure 3: Estimated gain image for plate A11.

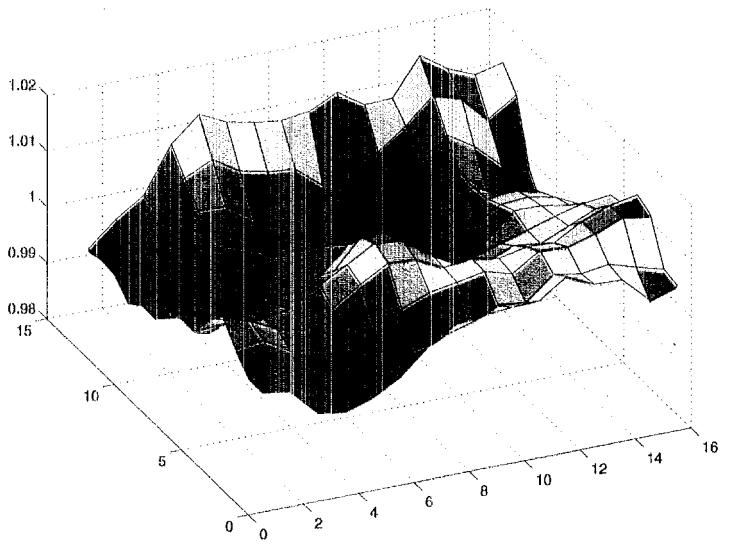

Figure 4: Estimated gain image for plate A27.

Plate	Runs	Spatial
A6	0.0109	0.0146
A11	0.0168	0.0191
A27	0.0056	0.0055
A31	0.0076	0.0073

Table 1: Comparison of spatial and across-run standard deviations.

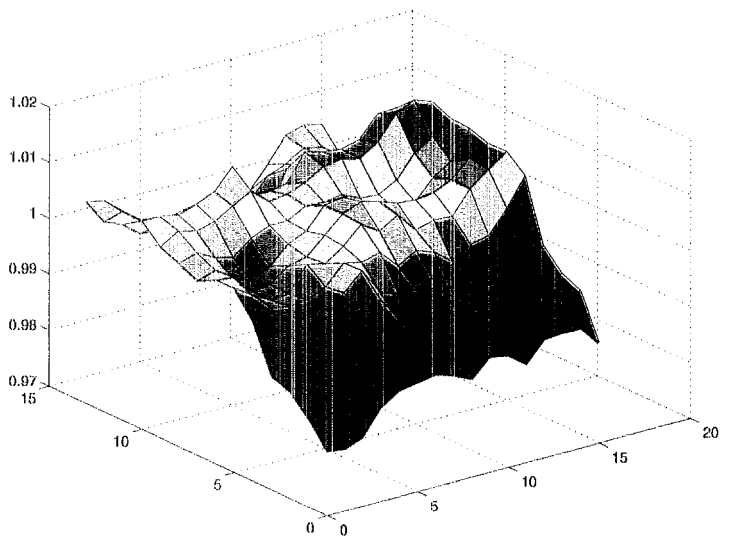

Figure 5: Estimated gain image for plate A31.

across-run variations as in Table 2. These values are sufficiently small to justify the model as a reasonable approximation to the data in the region of high beam intensity. However, the spatial variations in regions of high intensity are sufficiently small that there is need for the spatially varying gain model in this region. (Table 3 displays results for a restricted region of the same size, but of low beam intensity.) The reason for this behavior is unclear. While a decrease in the stability of the gain estimates due to noise effects is to be expected where the beam intensity is low, this does not explain the patterns of gain variation from one run to the next, which exhibit changing overall gradient rather than random fluctuations. These effects may be artifacts of the scanning process, or may represent unaccounted-for aspects of the plate-beam interaction, necessitating a more complex model than that explored above.

The effects of variations in gain coefficients in this model are briefly addressed in Appendix A.

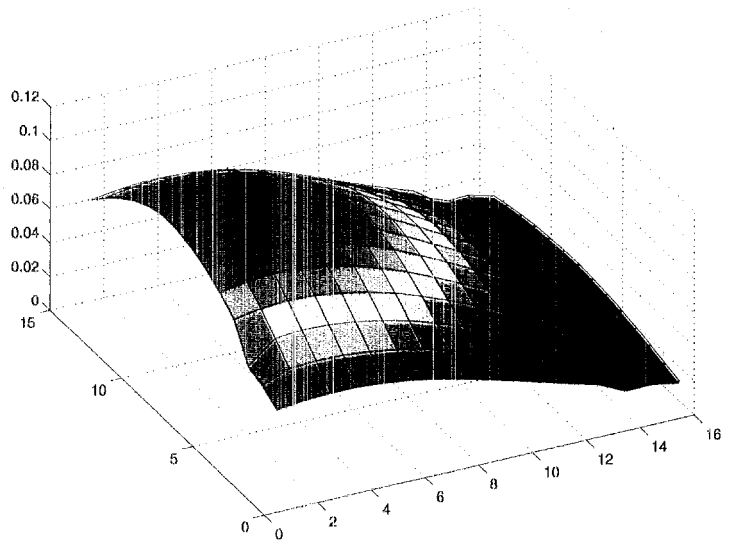

Figure 6: Estimated beam image for run 11451.

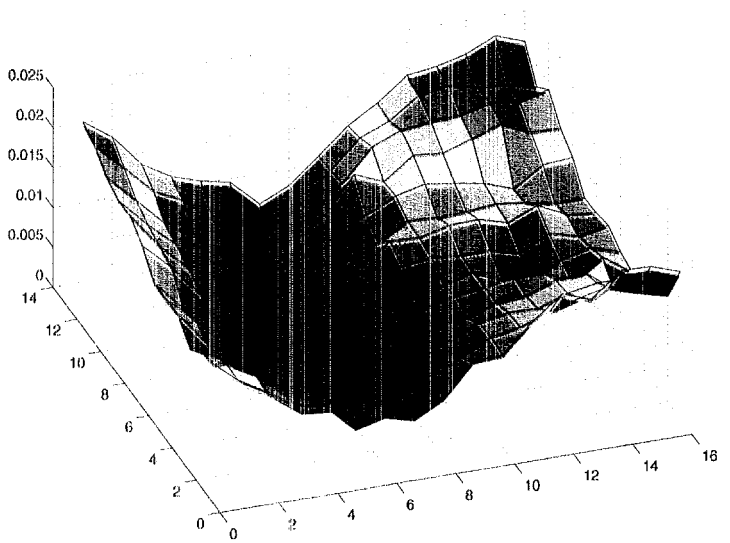

Figure 7: Comparison of spatial and across-run standard deviations for plate A6.

Plate	Runs	Spatial
A6	0.0057	0.0029
A11	0.0102	0.0032
A27	0.0028	0.0025
A31	0.0040	0.0028

Table 2: Comparison of spatial and across-run standard deviations for small region near peak of beam intensity.

Plate	Runs	Spatial
A6	0.0148	0.0065
A11	0.0345	0.0052
A27	0.0081	0.0033
A31	0.0126	0.0031

Table 3: Comparison of spatial and across-run standard deviations for small region of low beam intensity.

4 Variations Arising During Scanning

Distortion arising from minor variations in mounting of the plates on the scanner drum has been proposed as a mechanism behind the observed variability in recovered images. In order to measure this type of distortion, we exposed plates upon which a regular grid pattern had been inscribed or printed. Significant distortions in mounting on the scanning drum should give rise to distortions in the grid pattern in the scanned images; analysis of these distortions was expected to provide estimates of the variation in plate height above the scanning drum during scanning. Such height variation would (due to the particular nature of the laser scanning process) account for apparent gain variations across image plates.

As a result of the tight beam used to expose the plates, contrast was sufficiently poor near the edges of the plates that the grid pattern could not be reliably extracted. This prevented the intended plate height analysis from being performed. It should be noted, however, that visual inspection of the grid patterns of the scans revealed no discernible distortion.

5 Conclusion

The variable gain model of image plate response is attractive due to its simplicity, as well as the potential for correcting scanned images using measured gain images for each plate. While experimental data do not support this model as the only source of the observed variations, the approach utilized here is likely to be a valuable tool for any further investigations.

While it is possible to extend the model to include time-varying gain images for each plate, this would not be useful due to the impracticality of estimating the time variation for purposes of correcting scanned images. In addition, it appears to be an unlikely hypothesis; the plates are (from physical knowledge of their composition and function) not expected to retain state between erasures, and, if they did, such dependence on past history would be expected to be strongest in regions of highest radiation exposure, which is not in agreement with the observed behavior discussed in the previous section. A more likely explanation appears to be some unknown mechanism, arising during the scanning process, which causes variations in image gradient in regions of low image intensity. Given that across-run and spatial variations appear to be of similar magnitude, such a mechanism should be expected to be at least of the same significance as the spatial variation described by the model.

In summary, while our results suggest that the plate-scanner system responses varied (spatially) by up to 7%, the comparison of across plate and across run variation suggests that at most 50% of the observed variability is due to the static plate response variations, and that other mechanisms (quite likely linked to the scanning procedure) needed to be included in the model.

6 Recommendations for Future Work

The following experiments and analysis are suggested as profitable avenues for further work in characterizing the image plates:

- Repeat the main experiments described above using plates exposed using a high-intensity beam with a flatter profile. This would enable a more meaningful comparison of the across-runs and spatial variations in the plate gain model. It is also recommended that a greater number of plates be simultaneously exposed in a stack.

- Recorded exposure and scan times could be used, together with a model of the time-decay of the image on the plates, to estimate the $\alpha_{p,r}$ parameters in the model. This may possibly provide better results than the normalization approach used in the experiments described here.

- Expose a stack of plates (perhaps to an X-ray rather than a proton beam) together with a plate of standard single-use radiographic film. This film would be expected to provide an accurate beam image reference for comparison with the scans obtained from the plates.

- The optimization approach outlined in Section 3 should be further investigated as an alternative to averaging images from each plate in a stack to obtain a beam image estimate. In particular, the experiment should be repeated with a different object in the beam during each run, and the analysis should be repeated to compare the beam estimates B_r for each run.

- The analysis in this report is based on a somewhat *ad-hoc* deterministic model of the image acquisition system. A more detailed, physics-based statistical model of the noise at each stage of the system (plate activation by radiation, image decay before scanning, image detection by scanner, etc.) should be constructed.

- The grid-plate experiments should be repeated using a broader beam (or X-ray source) so that sufficient contrast is obtained across the whole image. Additional examination of the scanning process is necessary to understand the its role in the observed variation.

A Gain Coefficients and Reconstructions

An important question which we briefly address here is, "What effect does the uneven plate response have on reconstructions?" To answer this question, we first recall the relation between measured intensity I_m, beam intensity I_0, and object path length $\tilde{L} = \rho L/\lambda$ (ρ is material density, L is the length of the material in the beam line, and λ is the material's attenuation coefficient):

$$I_m = I_0 \exp(-\tilde{L}).$$

By inserting a multiplicative gain coefficient G, we obtain a modified relation

$$I_m = G I_0 \exp(-\tilde{L}).$$

Computing $\partial\tilde{L}/\partial G$ and normalizing by path length $\tilde{L}$ gives

$$\frac{\partial\tilde{L}}{\tilde{L}} = \frac{\partial G}{G}\tilde{L}^{-1},$$

which shows that the percent change in path length is given by the percent change in gain scaled by inverse path length. By ignoring gain (i.e. $G = 1.0$), we have

$$\frac{\partial \tilde{L}}{\tilde{L}} = \partial G \tilde{L}^{-1}.$$

This shows that for large path lengths, the effect of ignoring G will be small; for small path lengths, the effect will be substantial.

To make this more meaningful, consider a 5.0 cm length of Tungsten of density 19.3 g/cm^3, with $\lambda = 185.0$ g/cm^2; in this case, $\tilde{L} = 0.52$. So $\tilde{L}^{-1} = 1.9$, and we see that, according to our simple model, a deviation $\triangle G$ in gain from 1.0 will result in about a $2\triangle G$ percent change in path length.